Chinese Chemical Letters 33 (2022) 5023–5029

Contents lists available at ScienceDirect

Chinese Chemical Letters

journal homepage: www.elsevier.com/locate/cclet

Recent progress on two-dimensional materials confining single atoms for CO_2 photoreduction

Xianjin Shi[a,b,c], Leo N.Y. Cao[d,e], Meijuan Chen[f], Yu Huang[a,b,*]

[a] Key Laboratory of Aerosol Chemistry and Physics, State Key Laboratory of Loess and Quaternary Geology (SKLLQG), Institute of Earth Environment, Chinese Academy of Sciences, Xi'an 710061, China
[b] Center of Excellence in Quaternary Science and Global Change, Chinese Academy of Sciences, Xi'an 710061, China
[c] University of Chinese Academy of Sciences, Beijing 100049, China
[d] CAS Center for Excellence in Nanoscience, Beijing Key Laboratory of Micro-nano Energy and Sensor, Beijing Institute of Nanoenergy and Nanosystems, Chinese Academy of Sciences, Beijing 101400, China
[e] School of Nanoscience and Technology, University of Chinese Academy of Sciences, Beijing 100049, China
[f] School of Human Settlements and Civil Engineering, Xi'an Jiaotong University, Xi'an 710049, China

ARTICLE INFO

Article history:
Received 17 November 2021
Revised 11 December 2021
Accepted 25 January 2022
Available online 1 February 2022

Keywords:
CO_2 reduction
Photocatalyst
Single atom
2D materials
g-C_3N_4

ABSTRACT

Photoreduction of CO_2 into value-added products offers a promising approach to overcome both climate change and energy crisis. However, low conversion efficiency, poor product selectivity, and unclear mechanism limit the further advancement of CO_2 photoreduction. The development of two-dimensional (2D) materials and construction of single atom sites are two frontier research fields in catalysis. Combining the advantages of 2D materials and single atom sites is expected to make a breakthrough in CO_2 photoreduction. In this review, we summarized the design and application, proposed challenges and opportunities, and laid a foundation for further research and application of 2D materials confining single atoms (SACs@2D) for CO_2 photoreduction.

1. Introduction

In recent years, achieving carbon neutrality has attracted extensive attention in the media, politics, and science [1–3]. As a major greenhouse gas, the effective control of CO_2 emissions is critical to realizing carbon neutrality. If effective strategies to reduce CO_2 emissions are not taken, the steadily increasing concentration of carbon dioxide in the atmosphere will continue to increase the global average temperature, causing a series of natural disasters and extreme weather [3]. However, the increasing hunger for energy by an ever-growing human population is unceasing and there is no doubt that CO_2 emissions will not stagnate [4].

In nature, CO_2 can be converted into organic matter by plant photosynthesis, providing an effective way to solve the contradiction between the increase of energy consumption and the reduction of CO_2 emissions [5–10]. However, from a thermodynamic point of view, the reduction of CO_2 to CO, methane (CH_4), methanol (CH_3OH), formic acid (CHOOH), or other C2 productions are very unfavorable due to the high bond energy of C=O (750 kJ/mol) [11]. These processes, like the widely studied photocatalytic hydrogen evolution reaction (HER) and nitrogen reduction reaction (NRR) [12–14], require a certain amount of energy. Therefore, it is necessary to develop and use abundant "green" energy to catalyze the conversion of carbon dioxide. Being widely studied, photocatalysis using clean solar energy is one of the most effective methods to catalyze the recovery of CO_2 resources [15,16]. However, for photoreduction of CO_2 to value-add products, high criteria for photocatalyst design is required: (1) efficient conversion process, (2) good product selectivity, and (3) high stability [17]. As such, the design of photocatalyst is the key factor to achieving CO_2 reutilization *via* photocatalysis [18].

With high design criteria, single-atom catalysts (SACs) are the appropriate candidates for CO_2 reduction [19–21]. SACs have many advantages [22]: (1) unexpectedly high activity and selectivity due to its unsaturated coordination and tunable electronic structures; (2) the maximum atom utilization efficiency, resulting in the reduced cost, especially for precious metals; (3) well-defined active sites for mechanistic studies because they can bridge the gap between heterogeneous and homogeneous catalysis. Due to the unique advantages, numerous SACs were synthesized and studied in photocatalysis CO_2 reduction in recent years [18,23].

The general catalytic performance of SACs is determined by the selection of carrier materials because when the particle size is re-

* Corresponding author.
E-mail address: huangyu@ieecas.cn (Y. Huang).

https://doi.org/10.1016/j.cclet.2022.01.066
1001-8417/

duced to a single atom, the isolated atoms should be anchored on carrier materials that prevent aggregation due to an increase in surface free energy [18,24,25]. Therefore, to this end, supports in various carrier materials have been developed for anchoring single atoms, such as metal-containing materials (*e.g.*, TiO_2 [26], FeO_x [27], Mo_2S [28]) and metal-free materials (*e.g.*, graphene oxide [29], carbon nitride [30]).

Among the numerous carrier materials, two-dimensional (2D) materials are attractive candidates, which is the thickness of only one or a few atomic layers [11,15,31]. The unique physical and chemical structure of 2D material allows a higher density of single atoms. In addition, compared to block materials, 2D materials can create more unsaturated coordination centers, have unique electronic structures, and contain higher catalytic activity generally [32–34].

Combining the above-mentioned advantages of 2D materials and single atom sites, 2D materials confining single atoms (SACs@2D) have the following features [33,35,36]: (1) a large specific surface area to increase the metal single atom load and achieve 100% active sites exposure; (2) the energy band structure of 2D materials can be effectively adjusted by single atoms, and thus effectively improve the visible light response and photocatalytic CO_2 reduction performance; (3) the unsaturated coordination structure of SACs@2D benefits the adsorption and activation of CO_2, facilitating higher photocatalytic CO_2 reduction; (4) SACs@2D can be easily analyzed by advanced characterization techniques, providing convenience for theoretical research. Studies have shown that the single atomic sites on 2D materials are excellent CO_2 reduction sites [37–41]. Therefore, SACs@2D for CO_2 photoreduction is worthy of further study.

Although many reviews have summarized the synthesis, characterization, and application of 2D materials confining single atoms [31,33,42–44], a comprehensive overview of SACs@2D for the CO_2 photoreduction is missing, especially how single atoms are supported on 2D materials and the functions of single atoms sites for CO_2 reduction process. Therefore, in this review, the design of SACs@2D is first summarized, providing practical guidance for the design and synthesis of SACs@2D. Secondly, SACs@2D for photocatalytic CO_2 reduction is reviewed to provide a comprehensive understanding of the functions of single atomic sites. Finally, the major challenges and opportunities for further research and application of SACs@2D for CO_2 photoreduction are proposed. Thus, the research status and trends of SACs@2D in CO_2 photoreduction are fully understood, laying a foundation for the further application of SACs@2D for CO_2 photoreduction.

2. Single atoms supported on 2D nanomaterials

The key point of SACs synthesis is to anchor isolated atoms on the 2D carrier materials surface properly, because the prerequisite for the practical application of SACs is that the single atoms do not aggregate during the catalytic process, that is, the single atoms locate at the desired location without any significant migration [45]. However, preventing the aggregation of single atoms during preparation and catalysis is a great challenge [46]. Fortunately, there are many great significant progresses for 2D materials that support single atoms, providing theoretical guidance for the rational development of SACs@2D future. Taking typical 2D material g-C_3N_4 as an example [5,47–50], there are three main kinds of positions for anchoring single atoms: The pore structure, interlayer structure between two layers, and defect sites, as shown in Fig. 1. This section will review the suitable sites of 2D materials for confining single atoms.

2.1. Single atoms confined into pore structure

The intrinsic pore structure of some materials is a candidate to confine single atoms. For example, g-C_3N_4 is composed of tri-*s*-triazine rings, based on sp^2 hybridization of π conjugated graphite planes by alternating C and N connections [51–53]. The internal pore structure filled with six N atoms with lone-pair electrons is an ideal site for anchoring atoms to prevent them from aggregating.

In addition to the coordination on the original atoms of the pore structure, the heteroatoms on pore structure of 2D materials are also useful sites to support the single atom. For example, being widely studied, N heteroatom coordination metal single atoms (M-N_x) catalysts have shown their excellent catalytic activity for several catalytic reactions [54,55]. In addition to N atoms, O or P atoms are also alternative coordination heteroatoms. For example, Gao *et al.* reported single Co sites coordinated on the partially oxidized graphene nanosheets *via* a Co-O_3C configuration [22]. Moreover, Chu *et al.* also synthesized the sing Co atoms by coordinating Co above the void center of g-C_3N_4 by heteroatom P [56]. The strong ligand-metal coordination between single metal atoms and heteroatoms of 2D materials is beneficial for facile manipulation of loading sites.

One advantage of confining of single atom into the internal pore structure of 2D materials is to improve the light absorption capacity of 2D materials. For example, Xiong *et al.* synthesized a series of g-C_3N_4 inclusion Pt single atoms photocatalysts, in which Pt single atoms are confined to the "N pots" [57]. By incorporating a trace amount of Pt single atoms in the "N pots" of g-C_3N_4, the light absorption of g-C_3N_4 can be broadened to 900 nm by the metal-to-ligand charge transfer (MLCT). The MLCT mechanism also applies to non-noble metal Cu single atom confined in the internal pore structure. In addition to Pt and Cu atoms being confined to the internal pore structure, Fe and Zn atoms can also be incorporated into the g-C_3N_4 matrix, and it is found that the band gap of g-C_3N_4 becomes narrower with the introduction of Fe atoms [58].

In addition to light absorption properties, charge transfer properties can also be adjusted by introducing single atoms into the pore structure [59]. For example, Li *et al.* embedded isolated single Pt atoms on the top of the five-membered rings of g-C_3N_4 network [60]. The dispersion of single Pt atoms on g-C_3N_4 modulated the electronic structure and introduced the intrinsic change of the surface trap states, resulting in a nearly twofold decrease in average recovery lifetime of photon-generated carriers, suggesting that Pt

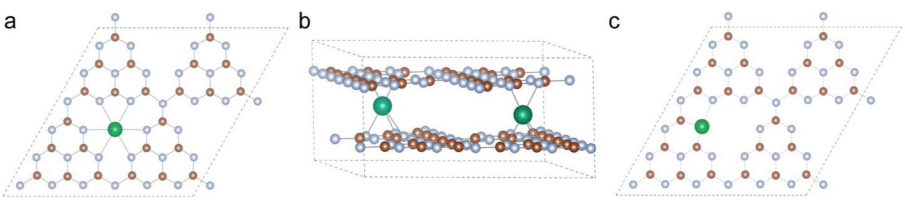

Fig. 1. Potential sites of single atom supported on g-C_3N_4: (a) pore structure; (b) interlayer space; (c) defect sites. Color codes: carbon is brown, oxygen is red, and a confined single atom is green.

single atoms provide more opportunities for photogenerated electrons to participate in photocatalytic reactions. The charge transfer channel can be constructed by placing the single atoms into the internal pore structure of g-C_3N_4, and the utilization rate of light can be improved.

Another advantage of confining single atom in the internal pore structure is to optimize the electronic structure and modify energy band levels. For example, M−N/C configurations can optimize the electronic structure and modify the band energy levels, because the electrons tend to transfer from the metal-sites to the N atoms *via* the strong interaction, resulting in the downshift of the valence band maximum (VBM) level. Inspired by the above phenomena, Su *et al.* modified the valence band structure of g-C_3N_4 by introducing Pt single atoms *via* a "high-valence metal single-atom confinement" strategy [61]. The hybridization of Pt 5d and N 2p downward shifts the VBM level of modified g-C_3N_4 by 0.26 V relative to bare g-C_3N_4, triggering a highly efficient photocatalytic water oxidation process.

Taken together, reasonably confined single atoms in the internal pore structure of 2D materials has the following functions: optimizing light absorption performance, improving charge transfer performance, adjusting band position, and providing the active sites for CO_2 photoreduction.

2.2. Single atoms confined in layer structure

The interlayer structure is also a candidate position for confining single atoms, because 2D materials are usually stacked together by weak van der Waals forces, which may prevent metal atoms from clustering [62]. Inspired by this, Cao *et al.* atomically dispersed Pd single atoms in both bridged sites of adjacent layers and surface-sites of g-C_3N_4 to accelerate charge separation [63]. Theoretical prediction and experiment characterizations reveal that single Pd atoms in bridged sites of adjacent layers provide directional charge-transfer channels. Such a unique structure efficiently boosts electron transport and separation. In addition to single Pd atoms, Cu single atoms can also be confined in the interlayer structure of g-C_3N_4 [64]. For example, Xiao *et al.* anchored Cu single atoms between g-C_3N_4 planes by intercalation of chlorophyll sodium copper ($C_{34}H_{31}CuN_4Na_3O_6$, CSC) into a supramolecular precursor. The single Cu atoms in two neighboring layers established Cu-N_4 charge transfer channels, which significantly improve the interlayer transfer of photogenerated charge carriers.

In addition to being confined in interlayers of the same material, single atoms can also be confined in the interfaces between 2D material and other semiconductor materials. For example, Zhao *et al.* prepared a series of composite photocatalysts by confining rare earth elements (Lu, Yb, Tm, Er, Ho, Dy, Gd, Eu, Nd, Pr, and La) single atoms onto the interface between g-C_3N_4 and CdS [65]. In these photocatalysts, CdS:Dy^{3+}/g-C_3N_4 is the best photocatalyst for CO_2 reduction. Further DFT calculation results show that single Dy atoms are suitable for electron transfer in the CdS/g-C_3N_4 due to the intermediate excited state energy level of Dy^{3+} located between the conduction bands of g-C_3N_4 and CdS. In addition, this strategy is also suitable for the synthesis of $SrTiO_3$:Er^{3+}/g-C_3N_4 composite catalysts [66]. The surface single Er atoms on $SrTiO_3$ facilitate the construction of charge transport channels between $SrTiO_3$ and g-C_3N_4, resulting in enhanced interfacial charge transfer and separation.

In general, the introduction of single atoms can enhance charge transfer in 2D material layers or interface between 2D material and other materials.

2.3. Single atoms confined into vacancy defects

Confined single atoms in defect sites, widely used in the synthesis of SACs, is also suitable for the synthesis of SACs@2D. For Example, Cao *et al.* designed and fabricated a series of single Au atoms supported on CdS with different types of vacancies (Fig. 2) [67]. For the sample of Au single atom supported on CdS with Cd vacancies ($Cd_{1-x}S$), the Cd vacancy electron paramagnetic resonance (EPR) signals decreased obviously after supporting single Au atoms, indicating that single Au atoms coverer part of Cd vacancies. Similarly, the authors also synthesized Au single-atom supported on CdS with S vacancies (CdS_{1-x}) samples. Interestingly, the types of vacancies for anchoring Au single atom highly affect the electron transfer direction.

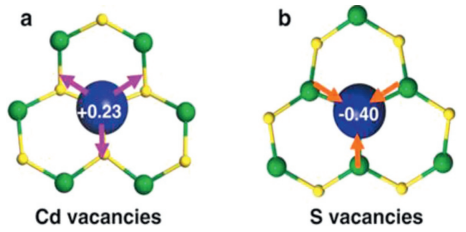

Fig. 2. Electron transfer between Au and CdS with different types of vacancies: (a) Cd vacancies; (b) S vacancies. Reprinted with permission [67]. Copyright 2021, Springer Nature.

A single atom will not only be confined in defects sites, it may also induce the formation of defective structures around it. For example, Zhang *et al.* found that single Ru atoms supported on MoS_2 induce phase transition of MoS_2 and generation of S vacancies, which efficiently tailors the electronic structure of MoS_2 [68].

In conclusion, single atoms supported on vacancy defects of 2D materials mainly play roles in regulating the band structure and providing the active site of 2D materials.

3. Photoreduction of CO_2 by SACs@2D

Upon identifying the design of SACs@2D, we are now in a position to decode the function of single atoms for CO_2 photoreduction. Generally, it is widely accepted that the photocatalytic CO_2 reactions are triggered by the photogenerated electrons on the surface of a semiconductor. For a SAC@2D catalysts, electrons in valence band of carrier material are excited into its conduction band when the photon energy is equivalent to or higher than its band gap energy. The excited electrons are transferred to the single atom sites to drive the CO_2 photoreduction reaction [69]. However, photocatalytic CO_2 reduction is a multiple proton-coupled electron transfer process with many intermediates, so the different numbers of transferred electrons and protons will form different reduction products. In addition, reduction potential determines whether the reaction can take place, which has strict requirements on the conduction band position of SACs@2D. Furthermore, for the multicarbon products, the difficulty of C–C coupling is another limiting factor. Up to now, the main products of photocatalytic CO_2 reduction are C1 products, including CO, CH_4, CH_3OH, and HCOOH, and only a few reported products were C2 or C2+ products. [11]. Therefore, the function of SACs@2D for photocatalytic CO_2 reduction will be reviewed in this section, and the typical applications of SACs@2D for photocatalytic CO_2 reduction are listed in Table 1 [22,35,67,70–81].

3.1. Noble metals-based SACs@2D

Due to the advantages of excellent catalytic activity and stability, the function of single sites in noble metals-based SACs@2D is worth studying [27,82–85]. Therefore, this part mainly introduces the functions of single noble metal sites in CO_2 reduction.

Table 1
Summary of various SAC@2D toward CO_2 reduction.

Photocatalyst	Test condition	Product	The function of single atom	Ref.
Au/g-C_3N_4	CO_2, H_2O, 300 W Xe arc lamp with an ultraviolet-cutoff filter	CO: 3.5 μmol g^{-1} h^{-1}, CH_3OH: 0.76 μmol g^{-1} h^{-1}, and CH_4: 0.12 μmol g^{-1} h^{-1}	Improve intermediate-adsorption ability, narrow band gap, and decrease carrier-recombination rate	[70]
Au/$Cd_{1-x}S$	CO_2, H_2O, A 300 W Xe arc lamp	CO: 32.2 μmol g^{-1} h^{-1}, CH_4: 11.3 μmol g^{-1} h^{-1}, and H_2: 7.9 μmol g^{-1} h^{-1}	Affect the direction of electron transfer, resulting in the accumulation of electrons in Cd vacancies	[67]
Ru/g-C_3N_4	CO_2, H_2O, 34 W blue LED light	1500 μmol/g (6 h of reaction time period)	Improves the light-harvesting capability,	[71]
Ti/g-C_3N_4	CO_2, TEOA, 300 W Xe lamp with a 420 nm cutoff filter	CO: 283.9 μmol g^{-1} h^{-1} and H_2: 115.3 μmol g^{-1} h^{-1}	Enhance the separation of photo-excited charges, improve visible light response	[72]
Fe/g-C_3N_4	CO_2, H_2O, 300 W xenon lamp	CO: 0.5 μmol g^{-1} h^{-1}	Increase the utilization of visible light, reduces the barrier of rate-limiting step	[73]
Co/g-C_3N_4	CO_2, TEOA, 300 W Xenon lamp	CO: 94.9 μmol g^{-1} h^{-1} and H_2: 56.4 μmol g^{-1} h^{-1}	Increase CO_2 adsorption, reduce the energy barrier of CO_2 hydrogenation activation	[74]
Co/Bi_3O_4Br	CO_2, H_2O, A 300 W Xe arc lamp	CO: 107.1 μmol g^{-1} h^{-1}	Favor the charge transition, carrier separation, CO_2 adsorption and activation	[75]
Co/black phosphorous	CO_2, TEOA, 300 W Xe-lamp with a 420 nm cut-off filter	CO: 88.6 μmol/h and H_2: 61.1 μmol/h (1.5 mg of catalyst powders)	Form additional charge transfer channel and active sites	[76]
Co/oxidized graphene	CO_2, TEOA, $[Ru(bpy)_3]Cl_2 \cdot 6H_2O$, 300 W Xe arc lamp	CO: turnover number reaches 678	Transfer photoexcited electrons	[22]
Co/MOF	CO_2, TEOA, A 300 W xenon arc lamp with a UV-cut filter,	CO: 200.6 μmol g^{-1} h^{-1} and CH_4: 36.76 μmol g^{-1} h^{-1}	Boost the electron–hole separation efficiency,	[77]
Ni/g-C_3N_4	CO_2, H_2O, Xenon arc lamp (visible-light)	CO: 8.6 μmol g^{-1} h^{-1} and CH_4: 0.5 μmol g^{-1} h^{-1}	Motivate interfacial carrier transfer, bind with CO_2 and enhance the rate-determining step of intermediates	[78]
Cu/g-C_3N_4	CO_2, H_2O, A 300 W Xe arc lamp	CO: 3.5 μmol g^{-1} h^{-1}, CH_3OH: 0.76 μmol g^{-1} h^{-1}, and CH_4: 0.12 μmol g^{-1} h^{-1}	Provide charge transfer pathways, activate CO_2 molecules and reduce the energy barrier	[79]
Mo/COFs	CO_2, H_2O, 300 W xenon arc lamp with a cut off filter of 420 nm	CO: 6.19 μmol g^{-1} h^{-1}, C_2H_4: 3.57 μmol g^{-1} h^{-1} and CH_4: 1.08 μmol g^{-1} h^{-1}	Enhance the adsorption and activation of CO, decrease energy barriers for the formation of C_2H_4	[80]
Er/g-C_3N_4	CO_2, H_2O, 300 W xenon arc lamp with a cut off filter of 420 nm	CO: 47.1 μmol g^{-1} h^{-1} and CH_4: 2.5 μmol g^{-1} h^{-1}	Activate the CO_2, improve the efficiency of light utilization	[81]
La/g-C_3N_4	CO_2, TEOA, Xenon arc lamp	CO: 92.0 μmol g^{-1} h^{-1} and CH_4: 5.6 μmol g^{-1} h^{-1}	Form charge-transfer channel and key active center for CO_2 activation, accelerated $COOH^*$ formation and CO desorption	[35]

The noble metals-based single sites determine the selectivity of the CO_2 photoreduction products. For example, Gao *et al.* investigated Pd/g-C_3N_4 and Pt/g-C_3N_4 for photoreduction of CO_2 by DFT calculations [86]. They found that the desorption of HCOOH from the Pd/g-C_3N_4 catalyst possesses the largest barrier on the entire reaction pathway (0.46 eV), while the desorption energy from the Pt/g-C_3N_4 catalyst is 1.06 eV, suggesting that the formation of HCOOH is unfavorable on the Pt/g-C_3N_4 catalyst. Similarly, Zhou *et al.* studied the noble metal (Rh, Pd, Ag, Ir, Pt, and Au) single atom supported on defective g-C_3N_4 for CO_2 photoreduction by DFT calculations [87]. They found that the noble metal single atom tends to be trapped at the N-vacancy sites of g-C_3N_4 rather than the surface internal pore structure. The N-vacancy-stabilized Pd single atom on g-C_3N_4 show the lowest energy barrier for HCOOH production.

In addition to affecting the selectivity of the product, noble metals-based single sites on SAC@2D can also improve the activity of the product. For example, as shown in Fig. 2, Cao *et al.* proposed a different mechanism for surface electron density modulation using single Au atoms supported CdS [67]. When electrons concentrate on vacancies rather than single Au atoms, the adsorption type of CO_2 changed from physical adsorption to chemical adsorption. The reason for this phenomenon is that the strong hybridization of Au 5d and S 2p orbits accelerates the photo-electrons transfer onto the surface. Therefore, lots of photoelectrons are transferred to the surface to participate in CO_2 reduction reaction and finally achieve efficient carbon dioxide reduction. Moreover, Xiang *et al.* synthesized Au single atoms on amino group-enriched graphitic carbon nitride through a mild urea reduction method [70]. For this catalyst, the CO and CH_4 yields over this Au single atom photocatalyst are 21.7 and 2.4 μmol/g after 2.5 h of visible-light illumination, which are about 1.97 and 4.15 times those of pure g-C_3N_4. This improved photocatalytic performance is ascribed to the improved intermediate-adsorption ability, narrowed band gap, and decreased carrier-recombination rate after the introduction of Au single atom. Note that the introduced amino group improves its CO_2 affinity and helps improve CO_2 reduction. In addition, Sharma *et al.* achieved efficient photocatalytic CO_2 reduction to CH_3OH by single Ru atoms supported on porous g-C_3N_4 catalysts with a high yield of 1500 μmol/g (6 h under visible light) [71]. Ru-N/C coordination structure can accelerate charge transfer and increase charge density of active sites, thus realizing the enhanced photocatalytic activity of Ru single atom modified g-C_3N_4 for the aqueous photoreduction of CO_2 to CH_3OH using water as the sacrificial agent.

To sum up, although the researches of noble metals-based SACs@2D for CO_2 photoreduction have made some progress in improving product yield and selectivity, many problems still need to be addressed. For Example, the application of noble metals-based SACs@2D catalysts in photocatalytic reduction of CO_2 is rarely reported with experimental validation but has been widely studied with other reactions, such as hydrogen production (Pt [57,60,88,89], Pd [90,91], Ag [59], and Rh [92]), NO oxidation (Pt [93,94] and Pd [95]), and acetylene hydrogenation (Pd [96] and Au [97]). The main reason why noble metals-based SACs@2D catalysts are rarely used in the photoreduction of CO_2 reaction in experiments is the competitive reaction of H_2 generation [98]. The H_2 production not only affects the utilization efficiency of photogenerated electrons but also limits the yield and selectivity of products such as CH_4. Therefore, in order to realize the application of noble metals-based SACs@2D catalysts

in CO_2 reduction reactions, the active sites must be reasonably modified.

3.2. Transition metal-based SACs@2D

When catalyst prices are considered, the substitution of cheap transition metals for noble metals is worth studying. Therefore, the function of transition metal single atom in SACs@2D for photoreduction CO_2 is summarized in this part.

The transition metal single atom with variable redox states is an excellent CO_2 photoreduction site. For example, Wang *et al.* synthesized Cu modified g-C_3N_4 by C-Cu-N_2 coordination structure *via* supramolecular preorganization with subsequent condensation [79]. In this photocatalyst, the variable-valence C-Cu-N_2 sites can provide effective charge transfer pathways reduce the energy barrier toward photocatalytic CO_2 reduction, as shown in Eqs. 1–7:

$$Cu/CN + h\nu \rightarrow Cu/CN(e^-) + Cu/CN\ (h^+) \quad (1)$$

$$Cu^+ + e^- \rightarrow Cu^0 \quad (2)$$

$$Cu^0 + CO_2 + 2H^+ \rightarrow [Cu^{2+}] + CO + H_2O \quad (3)$$

$$[Cu^{2+}] + Cu^0 \rightarrow 2Cu^+ \quad (4)$$

$$6Cu^0 + CO_2 + 6H^+ \rightarrow 6Cu^+ + CH_3OH + H_2O \quad (5)$$

$$8Cu^0 + CO_2 + 8H^+ \rightarrow 8Cu^+ + CH_4 + 2H_2O \quad (6)$$

$$2H_2O + 4h^+ \rightarrow 4H^+ + O_2 \quad (7)$$

Note that the mechanism mentioned above has a certain universality [99,100]. For example, Tang *et al.* demonstrated that single Ti-O species supported on g-C_3N_4 can convert CO_2 into CO by photoreduction [72]. The Ti^{4+} can be transformed to Ti^{3+} by the light-generated electrons under the visible light irradiation. Then, the reduced Ti^{3+} changes back to Ti^{4+} by one electron transfer to co-catalysts ($Co(bpy)_3{}^{2+}$) to convert CO_2 into CO.

Among the various function of transition metal single sites, CO_2 adsorption capacity is one of the most important functions. For example, Cheng *et al.* reported an unsaturated edge confinement strategy, that is, single Ni sites coordinated on the few layer g-C_3N_4 *via* a self-limiting method [78]. The obtained sample achieves a comparably high performance of CO_2 photoreduction to CO under visible light illumination (8.6 μmol g^{-1} h^{-1}), which is 7.8 times that of the unmodified few-layer g-C_3N_4. In this process, further mechanism studies showed that the introduction of unsaturated Ni-N coordination is beneficial to improving CO_2 adsorption capacity and facilitating photogenerated electrons transfer, thereby achieving the comparably high photocatalytic activity for converting CO_2 to CO. Moreover, Gong *et al.* synthesized g-C_3N_4 supported Co (Fe and Mn) single atom by one-step thermal treatment of Co-MOF (Fe-MOF and Mn-MOF) and urea in the air [101]. The obtained sample exhibits excellent performance for photocatalytic reduction of CO_2 to CO with a high CO evolution rate of 394.4 μmol g^{-1} h^{-1} under visible light irradiation with hole sacrificial agent (TEOA), which is over 80 times higher than that of unmodified g-C_3N_4 (4.9 μmol g^{-1} h^{-1}). Experiment results show that the main reasons for the great improved CO evolution rate are the improved CO_2 absorption ability and charge separation efficiency after the introduction of single Co atoms.

In addition to charge transfer and CO_2 adsorption, the transition metal single sites also greatly affect the activation of CO_2. For example, Li *et al.* prepared Cu single atoms supported on crystalline g-C_3N_4 nanorods catalyst by molten salts and reflux method [102]. For this catalyst, photoreduction of CO_2-to-CO is a favorable reaction than CO_2-to-CH_4 over single Cu sits, thus achieving the enhanced photocatalytic CO_2 reduction with near 100% selective CO_2 photoreduction to CO. In addition, Kou *et al.* introduced single MoN_2 sites into COF to construct Mo-COF materials and found that this active site can reduce CO_2 to C_2 product (C_2H_4) [80]. Further experiments and calculations show that the formation of C_2 is due to the reduction of the energy barrier for the formation of C_2H_4 by the introduction of Mo single atom.

In general, transition metal sites have multiple functions simultaneously. For example, Zhao *et al.* reported a single Fe atom supported on g-C_3N_4 catalyst for the CO_2 photoreduction with water as the sacrificial agent [73]. For this catalyst, experiment and DFT calculations results reveals that the function of single Fe atoms as follow: (1) activating CO_2 in the ground state; (2) increasing the rate constant of the limiting step; (3) providing the catalytic active center; (4) lowering the reaction barrier of the C–O bond cleavage in COOH. In other words, the above-mentioned advantages of single Fe atoms together improve the performance of photocatalytic reduction of CO_2.

In all, great progress has been made in developing the function of transition metal-based SACs@2D, but the role of some elements remains to be further studied. For example, some common single transition metal sites, such as Mn [103] and Zn [104], have been proved to be good choices for CO_2 reduction, but their support in 2D materials needs to be further studied.

3.3. Rare earth metal-based SACs@2D

Rare earth metal-based SACs@2D for CO_2 photoreduction is also worthy of study, and the reasons are listed below [105]. Firstly, the rare-earth elements are considered critical materials because of their optical, magnetic properties, and unique electronics, which are widely used in catalysis. Secondly, when rare earth metals are reduced to a single atomic scale, maximum utilization of metal elements can be achieved. In addition, atomic-scale rare-earth metals may have properties not found in their nanoscale homologues. Therefore, in this part, the function of rare earth metal single atom in SACs@2D for photoreduction CO_2 is reviewed.

The main function of single rare earth metal sites is to construct charge transport channels. For example, Chen *et al.* designed and synthesized single La atoms modified g-C_3N_4 with La-N charge-transfer bridge [35]. The La-modified g-C_3N_4 realized a high rate (92 μmol g^{-1} h^{-1}) and CO selectivity (80.3%) in photocatalytic CO_2 reduction. The experimental and DFT calculations results show that the variety of electronic states induced by 4f and 5d orbitals of the rare-earth La single atom and the p-d orbital hybridization of La-N atoms forms a charge transport channel, which is the key active sites for CO_2 activation.

Another function of the single rare earth element atom in SACs@2D is to build active sites for CO_2 photoreduction. For example, Ji *et al.* synthesized rare-earth element single atoms (Er) supported on g-C_3N_4 by a novel atom-confinement and coordination strategy [81]. With the increase of the amount of Er precursor, the dispersion density of single atoms can be tuned from the formation of a low-density Er single-atom catalyst with an Er mass loading of 2.5 wt% to a high-density Er single-atom catalyst with an Er mass loading of 20.1 wt%. In these two catalysts, the high-density Er single-atom catalyst shows higher catalytic performance, indicating that the active sites on the catalyst surface were effectively increased.

In another case, single rare earth metal atoms in SACs@2D have dual functions at the same time. For example, the dual functions of CO_2 molecular activation and charge transfer bridge for rare-earth element single atom systematically studied by Wang's groups [65,66,106]. Taking the Dy^{3+} single atom doped in the interface of CdS/g-C_3N_4 heterojunction as an example, this structure combines

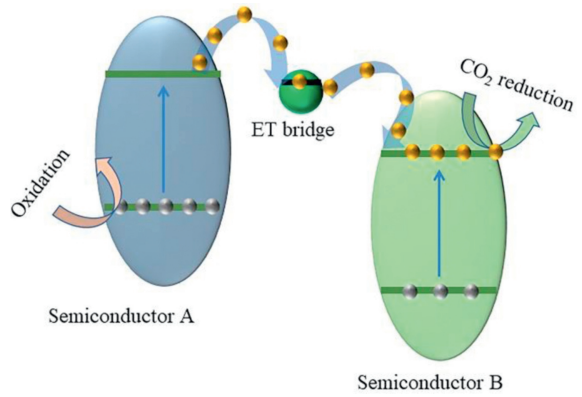

Fig. 3. The proposed mechanism for single rare-earth element atoms as ET bridges to promote charge separation.

the characteristics of rare-earth element single atom and the advantages of heterojunction [65]. In this photocatalyst, Dy^{3+} single atom is supported on the surface of CdS, so it also exists at the interface between CdS and g-C_3N_4. On the one hand, the intermediate excited state energy level of Dy^{3+} in the interface of CdS/g-C_3N_4 heterojunction can act as an electron transport bridge. On the other hand, the surface Dy^{3+} single atom changes the density of active sites, which can promote the absorption of CO_2. Under the dual functions of Dy single atom, the optimal catalyst realized an efficient photocatalytic reduction of CO_2 to CH_4. Guided by the same idea, this group synthesized dual functions Er single atom in Zn_2GeO_4/g-C_3N_4 heterojunction [106] and $SrTiO_3$/g-C_3N_4 heterojunction [66], and these rare-earth element single atom modified catalyst all achieved higher catalytic performance than that of pure g-C_3N_4. In such rare-earth element single atom supported on g-C_3N_4-based heterojunction (Fig. 3), the position of the 4f levels of rare earth elements as electron transport (ET) bridge is very closely related to the conduction band position of the heterojunction materials.

Over all, both theoretical and experimental studies on the loading of rare-earth elements on 2D materials for the photoreduction of CO_2 are still in the initial stage, which needs to be further studied to show the advantages of rare earth elements.

4. Conclusions and outlook

In summary, this review summarizes the design and functions of single atomic sites for CO_2 photoreduction of SACs@2D in recent years. The suitable sites of 2D materials for confining single atoms are internal pore structure, interlayer structure or interface, and vacancy defects or heteroatoms. Moreover, the functions of well-designed single atomic sites in CO_2 photoreduction includes enhanced light absorption, accelerated charge transfer, and improved adsorption and activation of CO_2.

Although the studies on SACs@2D for CO_2 photoreduction have achieved significant progress, a few research directions still deserve special attention:

(1) At present, the activity of photoreaction CO_2 over SACs@2D is still at a relatively low level compared to electrocatalysis and thermal catalysis, especially with water as the sacrificial agent. Therefore, the conversion rate of the product needs to be further improved. Similarly, how to improve product selectivity remains an important topic.

(2) The stability of the single atoms sites needs to be further studied, because single atoms tend to agglomerate into clusters or particles during synthesis and application process. In addition, the presence of other pollutants may also occupy the active site, leading to the loss of catalytic performance of SACs.

(3) The single atom active site on catalyst surface is a dynamic change process during CO_2 reduction, so more *in-situ* characterization should be conducted to study the changes of the single atom's physicochemical properties during CO_2 reduction. At present, most conclusions are based on DFT calculation results, so spectroscopic characterization or electron microscopy characterization is needed to give more intuitive evidence.

(4) At the present stage, most of the products of CO_2 photoreduction are C1 products. Some effective approaches can be taken into consideration to solve the above problems, such as introducing dual single-atom active sites and other reactive groups around the single atom sites, and enhancing the interaction between single atoms and their carrier interface.

Declaration of competing interest

The authors declare that they have no known competing financial interests or personal relationships that could have appeared to influence the work reported in this paper.

Acknowledgments

This work was supported by the Strategic Priority Research Program of the Chinese Academy of Sciences, China (Nos. XDA23010300 and XDA23010000), National Science Foundation of China, China (Nos. 51878644 and 41573138), the National Key Research and Development Program of China, China (No. 2016YFA0203000), and the Plan for "National Youth Talents" of the Organization Department of the Central Committee.

References

[1] Z. Jiang, X. Xu, Y. Ma, et al., Nature 586 (2020) 549–554.
[2] J.L. White, M.F. Baruch, J.E. Pander, et al., Chem. Rev. 115 (2015) 12888–12935.
[3] C. Hepburn, E. Adlen, J. Beddington, et al., Nature 575 (2019) 87–97.
[4] A. Rafiee, K.R. Khalilpour, D. Milani, M. Panahi, J. Environ. Chem. Eng. 6 (2018) 5771–5794.
[5] W. Tu, Y. Zhou, Z. Zou, Adv. Mater. 26 (2014) 4607–4626.
[6] U. Ulmer, T. Dingle, P.N. Duchesne, et al., Nat. Commun. 10 (2019) 1–12.
[7] O.K. Varghese, M. Paulose, T.J. LaTempa, C.A. Grimes, Nano Lett. 9 (2009) 731–737.
[8] S. Gong, G. Zhu, R. Wang, et al., Appl. Catal. B: Environ. 297 (2021) 120413.
[9] Y. Wang, Z. Zhang, L. Zhang, et al., J. Am. Chem. Soc. 140 (2018) 14595–14598.
[10] A. Li, Q. Cao, G. Zhou, et al., Angew. Chem. Int. Ed. 58 (2019) 14549–14555.
[11] D. Qin, Y. Zhou, W. Wang, et al., J. Mater. Chem. A 8 (2020) 19156–19195.
[12] P. Qiu, J. Wang, Z. Liang, et al., Chin. Chem. Lett. 32 (2021) 3501–3504.
[13] Z. Liang, Y. Xue, X. Wang, et al., Chem. Eng. J. 421 (2021) 130016.
[14] Z. Liang, X. Meng, Y. Xue, et al., J. Colloid Interface Sci. 598 (2021) 172–180.
[15] X. Jiao, K. Zheng, L. Liang, et al., Chem. Soc. Rev. 49 (2020) 6592–6604.
[16] T. Kong, Y. Jiang, Y. Xiong, Chem. Soc. Rev. 49 (2020) 6579–6591.
[17] T. Zhang, W. Lin, Chem. Soc. Rev. 43 (2014) 5982–5993.
[18] Y. Zhang, B. Xia, J. Ran, et al., Adv. Energy Mater. 10 (2020) 1903879.
[19] C. Gao, J. Low, R. Long, et al., Chem. Rev. 120 (2020) 12175–12216.
[20] S. Ji, Y. Chen, X. Wang, et al., Chem. Rev. 120 (2020) 11900–11955.
[21] Z. Li, S. Ji, Y. Liu, et al., Chem. Rev. 120 (2020) 623–682.
[22] C. Gao, S. Chen, Y. Wang, et al., Adv. Mater. 30 (2018) e1704624.
[23] Y.B. Lu, Z.H. Zhang, H.M. Wang, Y. Wang, Appl. Catal. B: Environ. 292 (2021) 120162.
[24] S. An, G. Zhang, T. Wang, et al., ACS Nano 12 (2018) 9441–9450.
[25] A. Wang, J. Li, T. Zhang, Nat. Rev. Chem. 2 (2018) 65–81.
[26] X. Zhou, Acta Physico-Chimica Sinica 37 (2021) 2008064.
[27] B. Qiao, A. Wang, X. Yang, et al., Nat. Chem. 3 (2011) 634–641.
[28] N. Aguilar, M. Atilhan, S. Aparicio, Appl. Surf. Sci. 534 (2020) 147611.
[29] M.B. Gawande, P. Fornasiero, R. Zboril, ACS Catal. 10 (2020) 2231–2259.
[30] C. Zupen, E. Vorobyeva, S. Mitchell, et al., Natl. Sci. Rev. 5 (2018) 642–652.
[31] P. Wang, D.Y. Zhao, L.W. Yin, Energy Environ. Sci. 14 (2021) 1794–1834.
[32] X. Jiao, X. Li, X. Jin, et al., J. Am. Chem. Soc. 139 (2017) 18044–18051.
[33] Y. Wang, J. Mao, X.G. Meng, et al., Chem. Rev. 119 (2019) 1806–1854.
[34] W. Shao, X.D. Zhang, Nanoscale 13 (2021) 7081–7095.
[35] P. Chen, B. Lei, X. Dong, et al., ACS Nano 14 (2020) 15841–15852.
[36] Q.S. Wang, D.F. Zhang, Y. Chen, et al., ACS Sustain. Chem. Eng. 7 (2019) 6430–6443.
[37] W. Zheng, Y. Wang, L. Shuai, et al., Adv. Funct. Mater. 31 (2021) 2008146.
[38] Y. Zhang, X. Wang, S. Zheng, et al., Adv. Funct. Mater. 31 (2021) 2104377.
[39] X. Wang, S. Feng, W. Lu, et al., Adv. Funct. Mater. 31 (2021) 2104243.
[40] J. Chen, Z. Li, X. Wang, et al., Angew. Chem. Int. Ed. 61 (2022) e202111683.
[41] S.F. Ji, Y. Qu, T. Wang, et al., Angew. Chem. Int. Ed. 59 (2020) 10651–10657.

[42] X.X. Zhao, K.P. Loh, S.J. Pennycook, J. Phys. Condens. Matter 33 (2021) 063001.
[43] Y.A. Zhou, J. Li, X.P. Gao, et al., J. Mater. Chem. A 9 (2021) 9979–9999.
[44] X. Li, X. Yang, J. Zhang, et al., ACS Catal. 9 (2019) 2521–2531.
[45] J. Jones, H. Xiong, A.T. DeLaRiva, et al., Science 353 (2016) 150–154.
[46] P. Zhou, F. Lv, N. Li, et al., Nano Energy 56 (2019) 127–137.
[47] Z. Wang, Y. Huang, L. Chen, et al., J. Mater. Chem. A 6 (2018) 972–981.
[48] S. Yin, J. Han, T. Zhou, R. Xu, Catal. Sci. Technol. 5 (2015) 5048–5061.
[49] K.S. Lakhi, D.H. Park, K. Al-Bahily, et al., Chem. Soc. Rev. 46 (2017) 72–101.
[50] S. Cao, J. Low, J. Yu, M. Jaroniec, Adv. Mater. 27 (2015) 2150–2176.
[51] X. Wang, K. Maeda, A. Thomas, et al., Nat. Mater. 8 (2009) 76–80.
[52] Y.C. Zhang, N. Afzal, L. Pan, et al., Adv. Sci. 6 (2019) 1900053.
[53] Z. Wang, M. Chen, Y. Huang, et al., Appl. Catal. B: Environ. 239 (2018) 352–361.
[54] E. Luo, Y. Chu, J. Liu, et al., Energy Environ. Sci. 14 (2021) 2158–2185.
[55] X.B. Zhu, B. Hu, C.X. Wang, et al., J. Catal. 391 (2020) 1–10.
[56] W. Liu, L.L. Cao, W.R. Cheng, et al., Angew. Chem. Int. Ed. 56 (2017) 9312–9317.
[57] Y.R. Li, Z.W. Wang, T. Xia, et al., Adv. Mater. 28 (2016) 6959–6965.
[58] X. Wang, X. Chen, A. Thomas, et al., Adv. Mater. 21 (2009) 1609–1612.
[59] X.H. Jiang, L.S. Zhang, H.Y. Liu, et al., Angew. Chem. Int. Ed. 59 (2020) 23112–23116.
[60] X.G. Li, W.T. Bi, L. Zhang, et al., Adv. Mater. 28 (2016) 2427–2431.
[61] H. Su, W. Che, F.M. Tang, et al., J. Phys. Chem. C 122 (2018) 21108–21114.
[62] Z. Zeng, Y. Su, X. Quan, et al., Nano Energy 69 (2020) 104409.
[63] S. Cao, H. Li, T. Tong, et al., Adv. Funct. Mater. 28 (2018) 1802169.
[64] X.D. Xiao, Y.T. Gao, L.P. Zhang, et al., Adv. Mater. 32 (2020) 2003082.
[65] Y. Zhao, Z. Han, G. Gao, et al., Adv. Funct. Mater. 31 (2021) 2104976.
[66] Q. Chen, G. Gao, Y. Zhang, et al., J. Mater. Chem. A 9 (2021) 15820–15826.
[67] Y. Cao, L. Guo, M. Dan, et al., Nat. Commun. 12 (2021) 1675.
[68] J.M. Zhang, X.P. Xu, L. Yang, et al., Small Methods 3 (2019) 1900653.
[69] X. Li, J.G. Yu, M. Jaroniec, X.B. Chen, Chem. Rev. 119 (2019) 3962–4179.
[70] Y.L. Yang, F. Li, J. Chen, et al., ChemSusChem 13 (2020) 1979–1985.
[71] P. Sharma, S. Kumar, O. Tomanec, et al., Small 17 (2021) 2006478.
[72] S.F. Tang, X.P. Yin, G.Y. Wang, et al., Nano Res. 12 (2019) 457–462.
[73] Z. Zhao, W. Liu, Y. Shi, et al., PCCP 23 (2021) 4690–4699.
[74] J. Fu, L. Zhu, K. Jiang, et al., Chem. Eng. J. 415 (2021) 128982.
[75] J. Di, C. Chen, S. Yang, et al., Nat. Commun. 10 (2019) 2840.
[76] X. Ren, L. Shi, Y. Li, et al., ChemCatChem 12 (2020) 3870–3879.
[77] H. Zhang, J. Wei, J. Dong, et al., Angew. Chem. Int. Ed. 55 (2016) 14308–14312.
[78] L. Cheng, H. Yin, C. Cai, et al., Small 16 (2020) 2002111.
[79] J. Wang, T. Heil, B. Zhu, et al., ACS Nano 14 (2020) 8584–8593.
[80] M. Kou, W. Liu, Y. Wang, et al., Appl. Catal. B: Environ. 291 (2021) 120146.
[81] S.F. Ji, Y. Qu, T. Wang, et al., Angew. Chem. Int. Ed. 59 (2020) 10651–10657.
[82] S. Sun, G. Zhang, N. Gauquelin, et al., Sci. Rep. 3 (2013) 1775.
[83] Y. Ren, Y. Tang, L. Zhang, et al., Nat. Commun. 10 (2019) 4500.
[84] K. Fujiwara, S.E. Pratsinis, Appl. Catal. B: Environ. 226 (2018) 127–134.
[85] N. Daelman, M. Capdevila-Cortada, N. Lopez, Nat. Mater. 18 (2019) 1215–1221.
[86] G.P. Gao, Y. Jiao, E.R. Waclawik, A.J. Du, J. Am. Chem. Soc. 138 (2016) 6292–6297.
[87] P. Zhou, Y.G. Chao, F. Lv, et al., Sci. Bull. 65 (2020) 720–725.
[88] Y.J. Cao, D.H. Wang, Y. Lin, et al., ACS Appl. Energy Mater. 1 (2018) 6082–6088.
[89] Y. Xue, Y.G. Lei, X.Y. Liu, et al., New J. Chem. 42 (2018) 14083–14086.
[90] X. Huang, H. Yan, L. Huang, et al., J. Phys. Chem. C 123 (2019) 7922–7930.
[91] N. Wang, J. Wang, J. Hu, et al., ACS Appl. Energy Mater. 1 (2018) 2866–2873.
[92] Z. Chen, Y. Bu, L. Wang, et al., Appl. Catal. B: Environ. 274 (2020) 119117.
[93] M. Ou, S.P. Wan, Q. Zhong, et al., Int. J. Hydrogen Energy 42 (2017) 27043–27054.
[94] S. Fang, X.R. Zhu, X.K. Liu, et al., Nat. Commun. 11 (2020) 1029.
[95] G. Liu, Y. Huang, H. Lv, et al., Appl. Catal. B: Environ. 284 (2021) 119683.
[96] X.H. Huang, Y.J. Xia, Y.J. Cao, et al., Nano Res. 10 (2017) 1302–1312.
[97] Z. Chen, Y. Chen, S. Chao, et al., ACS Catal. 10 (2020) 1865–1870.
[98] C. Dong, C. Lian, S. Hu, et al., Nat. Commun. 9 (2018) 1252.
[99] R. Li, W. Zhang, K. Zhou, Adv. Mater. 30 (2018) 1705512.
[100] S. Wang, J. Lin, X. Wang, Phys. Chem. Chem. Phys. 16 (2014) 14656–14660.
[101] Y. Gong, B. Shao, J. Mei, et al., Nano Res. 15 (2021) 551–556.
[102] Y. Li, B. Li, D. Zhang, et al., ACS Nano 14 (2020) 10552–10561.
[103] J. Yang, Z. Wang, J. Jiang, et al., Nano Energy 76 (2020) 105059.
[104] X. Cui, X. Dai, A.-.E. Surkus, et al., Chinese J. Catal. 40 (2019) 1679–1685.
[105] Z.M. Migaszewski, A. Galuszka, Crit. Rev. Env. Sci. Technol. 45 (2015) 429–471.
[106] Z. Han, Y. Zhao, G. Gao, et al., Small 17 (2021) 2102089.